Defects in coding joint formation in vivo in developing ATM-deficient B and T lymphocytes

Ching-Yu Huang,[1] Girdhar G. Sharma,[2] Laura M. Walker,[1] Craig H. Bassing,[3,4] Tej K. Pandita,[2] and Barry P. Sleckman[1]

[1]Department of Pathology and Immunology and [2]Department of Radiation Oncology, Washington University School of Medicine, St. Louis, MO 63110
[3]Department of Pathology and Laboratory Medicine, Children's Hospital of Philadelphia, University of Pennsylvania School of Medicine, Philadelphia, PA 19104
[4]Abramson Family Cancer Research Institute of the University of Pennsylvania Cancer Center, Philadelphia, PA 19104

Ataxia-telangiectasia mutated (ATM)–deficient lymphocytes exhibit defects in coding joint formation during V(D)J recombination in vitro. Similar defects in vivo should affect both T and B cell development, yet the lymphoid phenotypes of ATM deficiency are more pronounced in the T cell compartment. In this regard, ATM-deficient mice exhibit a preferential T lymphopenia and have an increased incidence of nontransformed and transformed T cells with T cell receptor α/δ locus translocations. We demonstrate that there is an increase in the accumulation of unrepaired coding ends during different steps of antigen receptor gene assembly at both the immunoglobulin and T cell receptor loci in developing ATM-deficient B and T lymphocytes. Furthermore, we show that the frequency of ATM-deficient αβ T cells with translocations involving the T cell receptor α/δ locus is directly related to the number of T cell receptor α rearrangements that these cells can make during development. Collectively, these findings demonstrate that ATM deficiency leads to broad defects in coding joint formation in developing B and T lymphocytes in vivo, and they provide a potential molecular explanation as to why the developmental impact of these defects could be more pronounced in the T cell compartment.

CORRESPONDENCE
Barry P. Sleckman:
Sleckman@
immunology.wustl.edu

Abbreviations used: AMuLV pre–B cell, v-abl–transformed mouse pre–B cell line; A-T, ataxia-telangiectasia; ATM, A-T mutated; BCR, B cell receptor; CE, coding end; DN, double negative; DP, double positive; DSB, double-strand break; JNK, c-Jun N-terminal kinase; LMPCR, ligation-mediated PCR; P8, probe 8; PR2, RAG-2 probe; PS6, SJA probe 6; RS, recombination signal; SE, signal end; WCP, whole chromosome paint.

The exons encoding the variable region of lymphocyte antigen receptor chains are assembled from V, J, and in some cases D gene segments through the process of V(D)J recombination (1). The V(D)J recombination reaction is initiated by the RAG-1 and -2 proteins (hereafter referred to as RAG). After synaptic complex formation, RAG introduces DNA double-strand breaks (DSBs) at the border of recombining gene segments and their flanking recombination signals (RSs) (2–4). The resulting pairs of blunt phosphorylated signal ends (SEs) and hairpin-sealed coding ends (CEs) are processed and joined into a signal joint and coding joint, respectively, by proteins of the nonhomologous end-joining pathway of DNA DSB repair (5).

The ataxia-telangiectasia (A-T) mutated (ATM) protein is a serine/threonine kinase activated early in the response to DNA DSBs (6–9). Mutations in the *ATM* gene cause A-T, a disease with lymphoid phenotypes that include lymphopenia and a predisposition to lymphoid malignancies (10, 11). Most lymphoid malignancies in A-T patients have karyotypic abnormalities with chromosome breakpoints clustering near antigen receptor genes (11). In addition, ~10% of nontransformed T cells from A-T patients have translocations or large inversions involving chromosomes containing TCR genes (chromosomes 7 and 14) (11).

Like A-T patients, ATM-deficient mice are lymphopenic, and they almost invariably die from thymic lymphomas with translocations involving the TCRα/δ locus by 3–6 mo of age (12–16). Thymocytes from ATM-deficient mice have an increased frequency of biallelic loss of distal Vα gene segments, and 11% of nontransformed αβ T cells in these mice have karyotypic abnormalities involving chromosome 14, which contains the TCRα/δ locus (17, 18). In ATM-deficient mice, the thymic lymphomas

The online version of this article contains supplemental material.

The Journal of Experimental Medicine

with TCRα/δ locus translocations are RAG dependent, and the T lymphopenia is partially rescued by TCR transgene expression (19–21). Collectively, these findings suggest that ATM functions during antigen receptor gene assembly.

RAG-induced DSBs are generated exclusively in developing lymphocytes at the G1 phase of the cell cycle (22, 23). ATM enforces the G1-S cell-cycle checkpoint through phosphorylation and stabilization of p53 and activation of the Chk2 kinase (7–9). Furthermore, p53 promotes apoptosis of cells with persistent unrepaired DSBs (7–9). In developing lymphocytes, ATM could therefore function primarily by activating the G1-S cell-cycle checkpoint in response to RAG-induced DSBs. However, mice deficient in either p53 or Chk2 are not lymphopenic and are not prone to lymphoid tumors with antigen receptor gene translocations, as are ATM-deficient mice (24, 25). Thus, ATM likely has distinct functions, in addition to its cell-cycle checkpoint/apoptotic activities, during V(D)J recombination.

Analyses of ATM-deficient cell lines did not reveal defects in V(D)J recombination of extrachromosomal plasmid substrates (26). However, ATM has been found to associate with RAG-induced DSBs generated at chromosomal loci (27). We recently analyzed ATM function during recombination of chromosomal substrates in v-abl–transformed mouse pre–B cell lines (AMuLV pre–B cells) that can be induced to undergo V(D)J recombination (28). Inhibition of the v-abl kinase with STI571 leads to G1 cell-cycle arrest, rapid induction of RAG gene expression, and, in wild-type AMuLV pre–B cells, robust rearrangement of chromosomally integrated retroviral recombination substrates (28). In contrast, although signal joint formation proceeds normally in ATM-deficient AMuLV pre–B cells, unrepaired CEs accumulate in these cells because of their loss from postcleavage complexes (28). Furthermore, these CEs are frequently aberrantly resolved as translocations or large chromosomal deletions or inversions (28). These results demonstrate that, in AMuLV pre–B cells, ATM performs an important, nonredundant function during coding joint formation.

Antigen receptor gene assembly at all loci in developing B and T cells relies on efficient coding joint formation, yet the T lymphopenia of ATM deficiency is much more profound than the B lymphopenia (12, 15). In addition, in developing ATM-deficient T cells, the most dramatic block in development is at the stage where TCRα chain genes are assembled and expressed (12). Finally, the antigen receptor gene translocations found in malignant and nonmalignant T cells from ATM-deficient mice primarily involve the TCRα/δ locus (18). Thus, whether ATM deficiency leads to broad defects in coding joint formation at all antigen receptor loci in vivo, as well as how these defects contribute to the lymphoid phenotypes of A-T, is not clear.

In this paper, using ligation-mediated PCR (LMPCR) and Southern blot approaches, we show that unrepaired CEs, but not SEs, accumulate at higher levels during the assembly of TCR and Ig genes in developing ATM-deficient T and B lymphocytes, respectively. Furthermore, we show that in ATM-deficient αβ T cells, the frequency of translocations and unrepaired DSBs involving the chromosome containing the TCRα/δ locus is related to the number of TCRα rearrangements that can be made in developing ATM-deficient thymocytes. These findings unequivocally demonstrate that ATM deficiency leads to broad defects in V(D)J recombination during both TCR and Ig gene assembly in developing B and T cells. Moreover, these results have important implications for the role of V(D)J recombination defects in the lymphoid phenotypes of A-T.

RESULTS

Accumulation of unrepaired TCR chain gene CEs in ATM-deficient thymocytes

Deficiencies in proteins required for normal coding or signal joint formation should result in an increased accumulation of unrepaired CEs or SEs, respectively, in developing lymphocytes. In $Atm^{-/-}$ mice, the most profound block in lymphocyte development is at the $CD4^+$:$CD8^+$ (double positive [DP]) stage of thymocyte development, where TCRα chain genes are assembled and expressed (12). To determine whether ATM functions during TCRα chain gene coding and/or signal joint formation, wild-type ($Atm^{+/+}$) and $Atm^{-/-}$ DP thymocytes were purified by flow cytometric cell sorting, and genomic DNA from these cells was assayed for Jα56 CEs and SEs by LMPCR (Fig. 1, A and B). To optimize for CE detection, genomic DNA was treated with a DNA polymerase to blunt DNA ends before linker ligation. Whereas the analyses of $Atm^{+/+}$ and $Atm^{-/-}$ DP thymocytes revealed nearly equivalent levels of Jα56 SEs, considerably higher levels of Jα56 CEs were detected in $Atm^{-/-}$ DP thymocytes (Fig. 1 B). Thus, in agreement with our findings in AMuLV pre–B cells, ATM deficiency leads to coding joint, but not signal joint, defects during TCRα chain gene assembly, as indicated by the increased accumulation of unrepaired Jα56 CEs in ATM-deficient DP thymocytes.

To determine whether ATM deficiency leads to coding joint defects at other TCR loci, we assayed for TCRβ and δ SEs and CEs in $Atm^{+/+}$ and $Atm^{-/-}$ thymocytes. TCRβ and δ chain genes are assembled in $CD4^-$:$CD8^-$ (double negative [DN]) thymocytes that express CD25 (29). $CD25^+$ DN thymocytes were purified from $Atm^{+/+}$ and $Atm^{-/-}$ mice by flow cytometric cell sorting, and genomic DNA from these cells was assayed for Jβ1.1, Jβ1.2, and Jδ1 CEs and SEs by LMPCR (Fig. 1, C–E). As both the TCRβ and δ loci have D gene segments, these analyses will also detect CEs generated by cleavage at DJβ1.1, DJβ1.2, and DJδ1 rearrangements (Fig. 1, C, D, F, and G).

$Atm^{+/+}$ and $Atm^{-/-}$ $CD25^+$ DN thymocytes had nearly equivalent levels of Jδ1 SEs (Fig. 1 E). These cells also had near equivalent levels of Jβ1.1, Jβ1.2, and 3′Dβ1 SEs (detected by the LMPCR for Jβ1 CEs; Fig. 1, C–E). However, as was observed for the TCRα locus, there were higher levels of unrepaired Jβ1.1, Jβ1.2, and Jδ1 CEs in $Atm^{-/-}$ DN thymocytes as compared with $Atm^{+/+}$ DN thymocytes (Fig. 1 E).

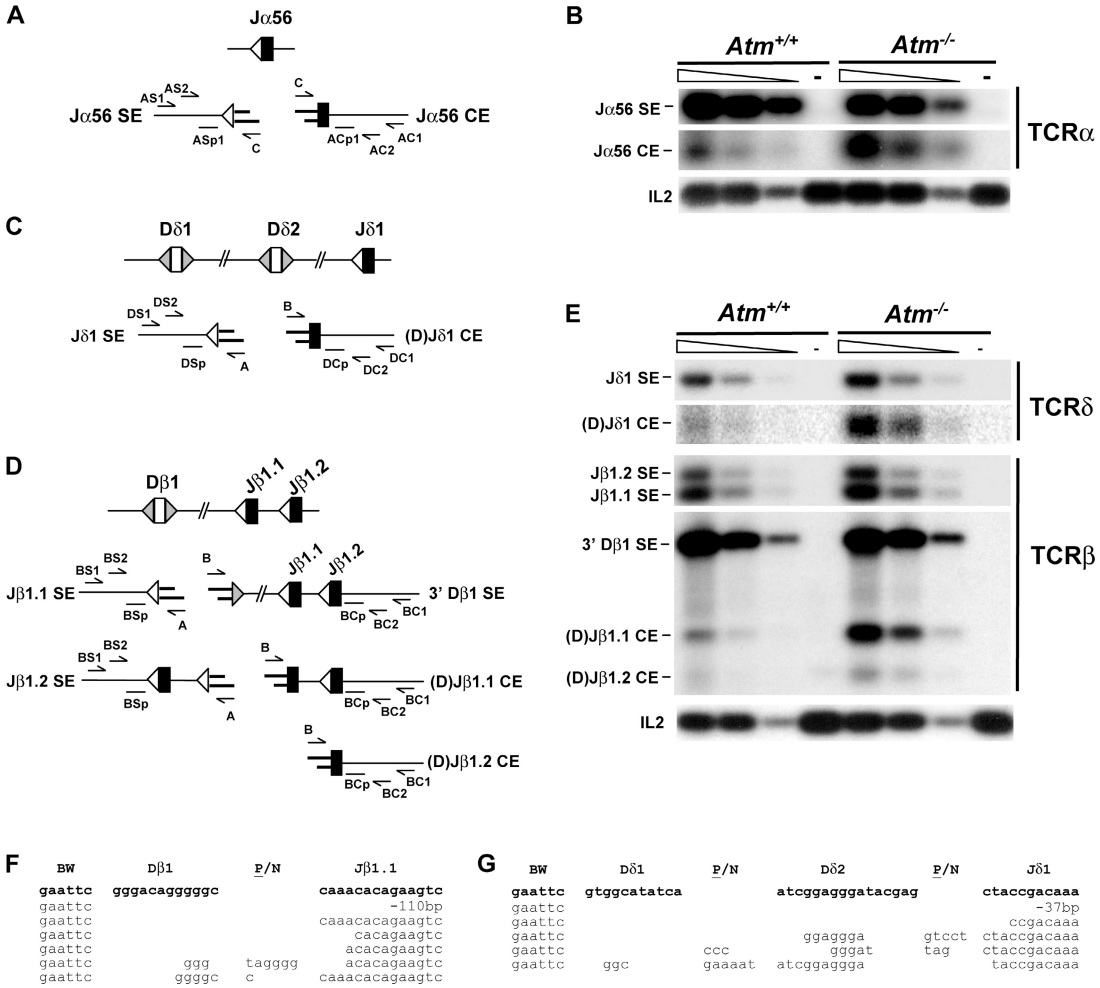

F

BW	Dβ1	P/N	Jβ1.1
gaattc	**gggacaggggc**		**caaacacagaagtc**
gaattc			-110bp
gaattc			caaacacagaagtc
gaattc			cacagaagtc
gaattc			acacagaagtc
gaattc	ggg	tagggg	acacagaagtc
gaattc	ggggc	c	caaacacagaagtc

G

BW	Dδ1	P/N	Dδ2	P/N	Jδ1
gaattc	**gtggcatatca**		**atcggagggatacgag**		**ctaccgacaaa**
gaattc					-37bp
gaattc					ccgacaaa
gaattc			ggaggga	gtcct	ctaccgacaaa
gaattc		ccc	gggat	tag	ctaccgacaaa
gaattc	ggc	gaaaat	atcggaggga		taccgacaaa

Figure 1. Increased TCR gene CE accumulation in developing ATM-deficient T cells. (A) Schematic of the Jα56 gene segment (closed rectangles) and its flanking RS (open triangles). Schematics of the CE/SE intermediates ligated to the ANC linker are shown. The approximate locations of oligonucleotides (arrows) used for LMPCR and probes (horizontal lines) are indicated. (B) LMPCR of genomic DNA from wild-type ($Atm^{+/+}$) and $Atm^{-/-}$ DP thymocytes for Jα56 CEs and SEs, as described in Materials and methods, using the primers and probes shown in A. Shown are fivefold serial dilutions of linker-ligated samples, as well as the no-ligase control (−). (C) Schematic of the TCRδ locus showing the Dδ1 and Dδ2 gene segments (open rectangles) and their flanking RSs (closed triangles), and the Jδ1 gene segment (closed rectangles) and its RS (open triangles). Schematics of different CE/SE intermediates ligated to the BW linker are shown. The approximate locations of oligonucleotides (arrows) used for LMPCR and probes (horizontal lines) are indicated. (D) Schematic of the TCRβ locus showing the Dβ1 gene segment (open rectangle) and its flanking RSs (closed triangles), the Jβ1.1 and Jβ1.2 gene segments (closed rectangles) and their RSs (open triangles), and different CE/SE intermediates ligated to the BW linker. The approximate locations of oligonucleotides (arrows) used for LMPCR and probes (horizontal lines) are indicated. (E) LMPCR of the $CD25^{+}$ DN thymocyte DNA for Jδ1, Jβ1.1, Jβ1.2, and Dβ1 SEs, and Jδ1, Jβ1.1, and Jβ1.2 CEs, as described in Materials and methods, using the primers and probes shown in C and D. Shown are fivefold serial dilutions of linker-ligated samples, as well as the no-ligase control (−). The IL-2 gene PCR is also shown as a DNA loading control. (F) Sequence analyses of Jβ1.1 CE LMPCR products. BW linker and germline Dβ1 and Jβ1.1 sequences are shown in bold. (G) Sequence analyses of Jδ1 CE LMPCR products. BW linker and germline Dδ1, Dδ2, and Jδ1 sequences are shown in bold. Palindromic (P) and nontemplated (N) nucleotide additions are indicated.

Sequence analyses revealed that the Jβ1.1 and Jδ1 LMPCR products were heterogeneous, and several included Dβ and Dδ gene segment nucleotides, respectively (Fig. 1, F and G). Collectively, these data demonstrate that ATM deficiency leads to broad defects in coding joint formation during different steps (V to J, D to J, and V to DJ) of TCR gene assembly at multiple loci (TCRα, β, and δ) in developing thymocytes.

Defects in coding joint formation in developing ATM-deficient B cells

To determine whether ATM functions during coding and/or signal joint formation at Ig loci in developing B cells, IgH and IgLκ chain gene CEs and SEs were assayed by LMPCR of genomic DNA from $Atm^{+/+}$ and $Atm^{-/-}$ bone marrow (Fig. 2).

As was observed for TCR gene rearrangement, analyses of $Atm^{+/+}$ and $Atm^{-/-}$ bone marrow revealed similar levels

of JH1 SEs at the IgH locus and Jκ1 SEs at the IgLκ locus (Fig. 2 C). However, considerably higher levels of JH1 and Jκ1 CEs were detected in $Atm^{-/-}$ bone marrow (Fig. 2 C). Sequence analyses demonstrated that the LMPCR products were heterogeneous and were generated by linker ligation to DJH1, JH1, and Jκ1 CEs (unpublished data). Collectively, these data demonstrate that developing ATM-deficient B cells also have defects in coding joint formation, as indicated by an increased accumulation of unrepaired CEs during DH to JH and VH to DJH rearrangements at the IgH locus and Vκ to Jκ rearrangements at the IgLκ locus.

Quantitative assessment of CE accumulation in ATM-deficient thymocytes

The LMPCR analyses demonstrate that unrepaired CEs exist at higher levels in developing $Atm^{-/-}$ lymphocytes. However, this type of analysis cannot be used to determine the fraction of alleles that have unrepaired CEs, which is needed to assess the potential developmental impact of coding joint defects in ATM-deficient mice. As most antigen receptor loci contain many gene segments, it would be difficult to quantitatively assay the total accumulation of unrepaired CEs at a specific locus. Accordingly, we generated $Atm^{+/+}$ and $Atm^{-/-}$ mice that were homozygous for the TCRα^{sJ} allele ($TCR\alpha^{sJ/sJ}$:$Atm^{+/+}$ and $TCR\alpha^{sJ/sJ}$:$Atm^{-/-}$ mice, respectively; Fig. 3 A) (30). The wild-type TCRα locus (TCRα^{+}) has ∼100 Vα and 61 Jα gene segments, and all Vα to Jα rearrangements occur by deletion (31). The TCRα^{sJ} allele is identical to the wild-type TCRα locus except that the 61 Jα gene segments have been replaced with 2 Jα gene segments (Jα61 and Jα56) through a multistep gene-targeting approach (Fig. 3 A) (30). Thus, rearrangement of any of the ∼100 Vα gene segments on the TCRα^{sJ} allele must occur to 1 of the 2 closely linked (0.4 kb) Jα gene segments.

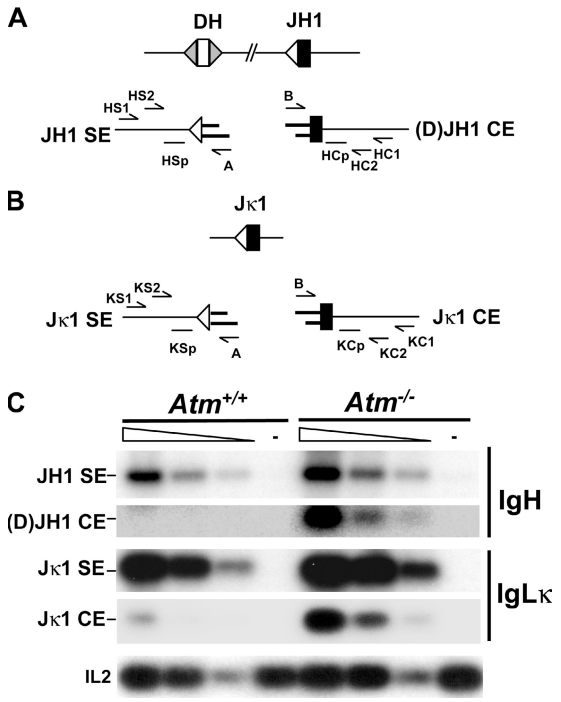

Figure 2. Increased IgH and IgLκ CE accumulation in developing ATM-deficient B cells. (A) Schematic of the IgH locus showing a DH (open rectangle) gene segment and its flanking RSs (closed triangles), the JH1 gene segment (closed rectangles) and its RS (open triangles), CE/SE intermediates ligated to the BW linker, and oligonucleotides used for LMPCR. (B) Schematic of the Jκ1 gene segment (closed rectangles), CE/SE intermediates ligated to the BW linker, and oligonucleotides used for LMPCR. Schematics of CE/SE intermediates ligated to the BW linker are shown. The approximate locations of oligonucleotides (arrows) used for LMPCR and probes (horizontal lines) are indicated. (C) LMPCR for JH SE/CE and Jκ1 SE/CE in $Atm^{+/+}$ and $Atm^{-/-}$ bone marrow DNA, as described in Materials and methods, using the primers and probes shown in A and B. Shown are fivefold serial dilutions of linker-ligated samples, as well as the no-ligase control (−). The IL-2 gene PCR is also shown as a DNA loading control.

Southern blot analyses of TCRα signal and coding joints in TCRα$^{sJ/sJ}$ thymocytes should reveal heterogeneously sized fragments, as any 1 of the ∼100 Vα gene segments can rearrange to either of the 2 Jα gene segments in each individual cell. However, as all of these rearrangements will involve the generation of a SE and CE at one of the two closely linked Jα gene segments, we reasoned that these DNA ends may be detected as discrete fragments by Southern blotting.

Southern blot analyses of $TCR\alpha^{sJ/sJ}$:$Atm^{+/+}$ and $TCR\alpha^{sJ/sJ}$:$Atm^{-/-}$ thymocyte DNA digested with two restriction enzymes and hybridized to probe 8 (P8; Fig. 3 B) upstream of Jα61 revealed fragments of the expected size for germline TCRα^{sJ} alleles and many different-sized fragments generated by heterogeneous signal joint formation (Fig. 3 C). Importantly, prominent fragments of the expected size for Jα61 SEs were also observed at equal intensities in $TCR\alpha^{sJ/sJ}$:$Atm^{+/+}$ and $TCR\alpha^{sJ/sJ}$:$Atm^{-/-}$ thymocyte DNA (Fig. 3 C). These fragments were sensitive to exonuclease V digestion, further demonstrating that they likely represent unrepaired SEs (Fig. 3, D and E). Notably, prominent fragments of the expected size for Jα56 SEs were not detected (Fig. 3 C). This would be expected if, like the wild-type TCRα locus, rearrangement of the TCRα^{sJ} allele is ordered, with the more 5′ Jα gene segment (Jα61) being used before the 3′ Jα gene segment (Jα56) (32–34). In this regard, P8 would not detect Jα56 SEs on TCRα^{sJ} alleles that had undergone a Vα to Jα61 rearrangement, which deletes the P8-hybridizing region from the chromosome (Fig. 3 B). LMPCR analyses, however, confirmed that Jα56 SEs are present at nearly equivalent levels in $TCR\alpha^{sJ/sJ}$:$Atm^{+/+}$ and $TCR\alpha^{sJ/sJ}$:$Atm^{-/-}$ thymocytes (Fig. 3 F).

Jα56 and Jα61 CEs were assayed by Southern blot analysis using two different restriction enzymes and a probe (CαI; Fig. 4 A) downstream of the Jα56 gene segment (Fig. 4 A). In addition to fragments expected for heterogeneous VJα coding joints and germline TCRα^{sJ} alleles, these analyses revealed a novel fragment of expected size for unrepaired Jα56 CEs in $TCR\alpha^{sJ/sJ}$:$Atm^{-/-}$ thymocyte DNA (Fig. 4, A and B). This fragment was not present in $TCR\alpha^{sJ/sJ}$:$Atm^{+/+}$ thymocyte DNA (Fig. 4 B). Furthermore, hybridization with SJA probe 6 (PS6; Fig. 4 A) to a region between the Jα56 and Jα61 gene segments revealed a fragment of expected size for

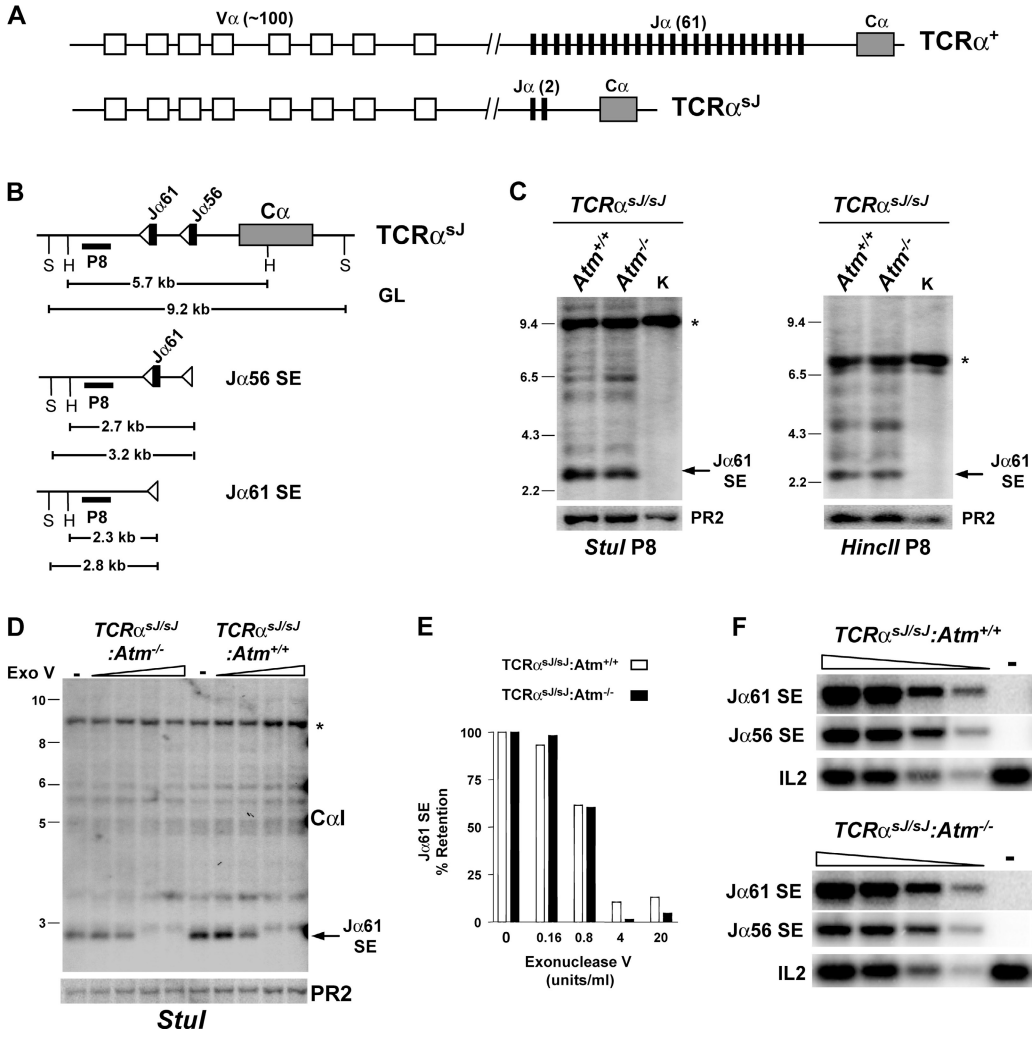

Figure 3. Equivalent TCRα^{sJ} locus SE accumulation in *Atm*$^{+/+}$ and *Atm*$^{-/-}$ thymocytes. (A) Schematics of the wild-type TCRα^{+} and TCRα^{sJ} loci. The Vα (open rectangles) and Jα (closed rectangles) gene segments are shown, as is the TCRα constant region gene (Cα; gray rectangles). The number in parenthesis indicates the number of Jα segments in the locus. (B) Southern blot analysis strategy. The relative positions of the *HincII* (H) and *StuI* (S) sites and P8 are shown. Fragment sizes generated by germline TCRα^{sJ} alleles and Jα56 and Jα61 SEs are indicated. The schematics are not drawn to scale. (C) Southern blot analyses of total thymocyte DNA and kidney DNA (K) digested with either *StuI* or *HincII* and hybridized to P8. Hybridization to PR2 is shown as a DNA loading control. The fragment corresponding to the germline TCRα^{sJ} allele is indicated by the asterisk. The fragments corresponding to the Jα61 SE are also indicated (arrows). The molecular mass markers (in kb) are indicated. (D and E) Thymocyte genomic DNA was digested in the absence (−) or in the presence of increasing concentrations of exonuclease V (ExoV) before digestions with *StuI* and hybridization to P8 (D). The fragment corresponding to the germline TCRα^{sJ} allele is indicated by the asterisk. Retention of the Jα61 SE band (arrow) in exonuclease V–treated samples was quantified as described in Materials and methods (E). (F) LMPCR analysis of Jα56 and Jα61 SEs, as described in the Materials and methods. Shown are fivefold serial dilutions of linker-ligated samples, as well as the no-ligase control (−). IL-2 gene PCR is also shown as a DNA loading control.

Jα61 CEs only in *TCRα*$^{sJ/sJ}$*:Atm*$^{-/-}$ thymocytes (Fig. 4, A and B). Quantification of these novel fragments, as described in Materials and methods, revealed that 17% (8% Jα56 and 9% Jα61) of TCRα^{sJ} alleles in *TCRα*$^{sJ/sJ}$*:Atm*$^{-/-}$ thymocytes have unrepaired CEs. LMPCR analyses confirmed the increased accumulation of Jα56 and Jα61 CEs in *TCRα*$^{sJ/sJ}$*:Atm*$^{-/-}$ thymocytes (Fig. 4 C).

Treatment of genomic DNA with exonuclease V led to a 40% loss in hybridization of the Jα56 CE fragment (Fig. 4, D and E). Treatment of genomic DNA with mung bean nuclease, which opens hairpin-sealed CEs, before exonuclease V treatment led to a nearly complete loss of hybridization (Fig. 4, F and G). Thus, approximately half of the unrepaired CEs in ATM-deficient thymocytes are hairpin sealed, raising the possibility that ATM may have some function in the hairpin opening process. Collectively, these data demonstrate that a substantial fraction of *TCRα*$^{sJ/sJ}$*:Atm*$^{-/-}$ thymocytes have unrepaired Jα CEs that exist in either hairpin-sealed or opened configurations.

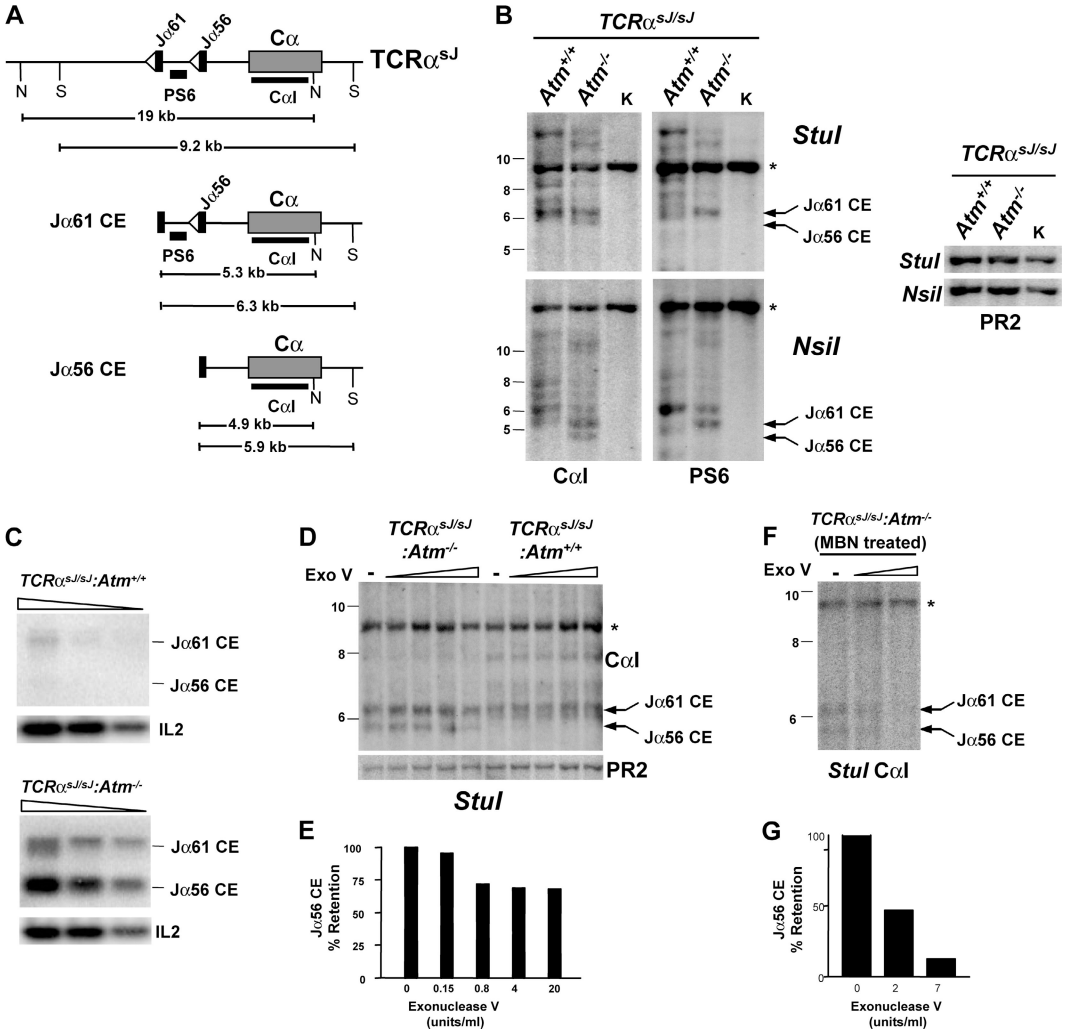

Figure 4. Increased TCRα^{sJ} locus CE accumulation in *Atm*$^{-/-}$ thymocytes. (A) Southern analysis strategy showing the relative positions of the *NsiI* (N) and *StuI* (S) sites, PS6, and the CαI probe. Fragment sizes generated by germline TCRα^{sJ} alleles and Jα56 and Jα61 CEs are indicated. The schematics are not drawn to scale. (B) Southern blot analyses of total thymocyte DNA and kidney DNA (K) digested with either *NsiI* or *HincII* and hybridized to the CαI probe or PS6. Bands corresponding to Jα61 and Jα56 CEs are indicated (arrows). The band corresponding to the germline fragment is indicated by an asterisk. Hybridization of *StuI* and *NsiI* digested DNA to PR2 is shown as a DNA loading control. The molecular mass markers (in kb) are indicated. (C) LMPCR analysis of Jα56 and Jα61 CEs, as described in Materials and methods. Shown are fivefold serial dilutions of linker-ligated samples. IL-2 gene PCR is also shown as a DNA loading control. (D and E) Exonuclease V sensitivity of Jα56 CEs was assayed by hybridizing the membrane from Fig. 3D to the CαI probe. Bands corresponding to the Jα61 and Jα56 CEs are indicated (arrows). The band corresponding to the germline TCRα^{sJ} allele is indicated by an asterisk. The positions of the molecular mass markers (in kb) are indicated (D). Retention of the Jα56 CE band in exonuclease V–treated samples was quantified as described in Materials and methods (E). (F and G) *TCRα*$^{sJ/sJ}$*:Atm*$^{-/-}$ thymocyte DNA was treated with mung bean nuclease followed by exonuclease V before digestion with *StuI* and hybridization to the CαI probe, as described in Materials and methods. Fragments corresponding to Jα61 and Jα56 CEs are indicated (arrows). The fragment corresponding to the germline TCRα^{sJ} allele is indicated by an asterisk (F). Retention of the Jα56 CE band in samples treated with mung bean nuclease and exonuclease V was quantified as described in Materials and methods (G).

Reduced chromosome 14 breaks and translocations in *TCRα*$^{sJ/sJ}$*:Atm*$^{-/-}$ αβ T cells

ATM-deficient mice have increased numbers of nonmalignant αβ T cells with karyotypic abnormalities involving chromosome 14, which contains the TCRα/δ locus (11, 18). Our analyses of V(D)J recombination in *Atm*$^{-/-}$ AMuLV pre–B cells demonstrated that unrepaired CEs are frequently resolved aberrantly as translocations or large chromosomal deletions or inversions (28). In DP thymocytes, each TCRα allele usually undergoes several Vα to Jα rearrangements (see Discussion). Thus, the increased frequency of chromosome 14 aberrations observed in *Atm*$^{-/-}$ αβ T cells could be due, in part, to the cumulative risk that any one of these multiple rearrangements would be aberrantly resolved.

To investigate this possibility, cytogenetic analyses were performed on metaphases from proliferating *TCRα*$^{+/+}$*:Atm*$^{-/-}$

and $TCR\alpha^{sJ/sJ}$:$Atm^{-/-}$ αβ T cells, as described in Materials and methods. As discussed above, the TCRα^{sJ} allele can undergo only two Vα to Jα rearrangements, whereas the wild-type TCRα allele has the potential to undergo many more Vα to Jα rearrangements. Metaphases were hybridized with red whole chromosome paint (WCP) for chromosome 14 and green WCP for chromosome 15, which serves as a control as it does not contain antigen receptor loci. Chromosome 14 or 15 aberrations were not observed in $TCR\alpha^{+/+}$:$Atm^{+/+}$ or $TCR\alpha^{sJ/sJ}$:$Atm^{+/+}$ αβ T cells (Fig. 5). In close agreement with published studies, 8% of $TCR\alpha^{+/+}$:$Atm^{-/-}$ αβ T cells had chromosome 14 aberrations (Fig. 5) (18). In contrast, only 4% of $TCR\alpha^{sJ/sJ}$:$Atm^{-/-}$ αβ T cells had chromosome 14 aberrations (Fig. 5). Notably, the chromosome 14 aberrations in $TCR\alpha^{+/+}$:$Atm^{-/-}$ and $TCR\alpha^{sJ/sJ}$:$Atm^{-/-}$ αβ T cells were equally divided between translocations and replicated chromosomal breaks (Fig. 5 C). From these analyses, it is not possible to determine whether the observed chromosome 14 aberrations are derived from TCRα or TCRδ chain gene rearrangements. However, the TCRδ locus is unaltered on the TCRα^{sJ} allele, making it unlikely that the change in the frequency of chromosome 14 aberrations is caused by differences in the TCRδ locus–derived translocations. Collectively, these findings demonstrate that ATM-deficient mice with TCRα alleles that undergo fewer Vα to Jα rearrangements have fewer peripheral αβ T cells with chromosome 14 aberrations. In addition, they suggest that RAG-induced DSBs generated in ATM-deficient thymocytes can persist unrepaired, as indicated by the chromosome 14 breaks in mature ATM-deficient αβ T cells.

DISCUSSION

In this paper, we show that ATM deficiency leads to broad defects in coding joint formation in vivo, as indicated by the increased accumulation of unrepaired CEs at Ig and TCR loci in developing ATM-deficient B and T lymphocytes. In contrast, unrepaired SEs were found at nearly equivalent levels when comparing wild-type and ATM-deficient lymphocytes, demonstrating that ATM does not perform an essential nonredundant function during signal joint formation.

The structure of most antigen receptor loci prohibits the simple quantitative assessment of the fraction of loci with unrepaired CEs or SEs. However, through Southern blot analysis of ATM-deficient thymocytes with a modified TCRα locus (TCRα^{sJ}), we show that 17% of alleles have unrepaired Jα CEs (Fig. 4 B). That 2% of peripheral $TCR\alpha^{sJ/sJ}$:$Atm^{-/-}$ αβ T cells have chromosome 14 breaks suggests that at least some Jα CEs generated in ATM-deficient DP thymocytes can persist unrepaired for the period of time it takes these cells to be positively selected and released into the periphery (Fig. 5). These findings are in remarkable agreement with analyses of ATM-deficient AMuLV pre–B cells, which revealed that 10–20% of retroviral recombination substrates develop persistent unrepaired CEs after induction of V(D)J recombination (28). Several lines of evidence, including interphase fluorescent in situ hybridization, revealed that

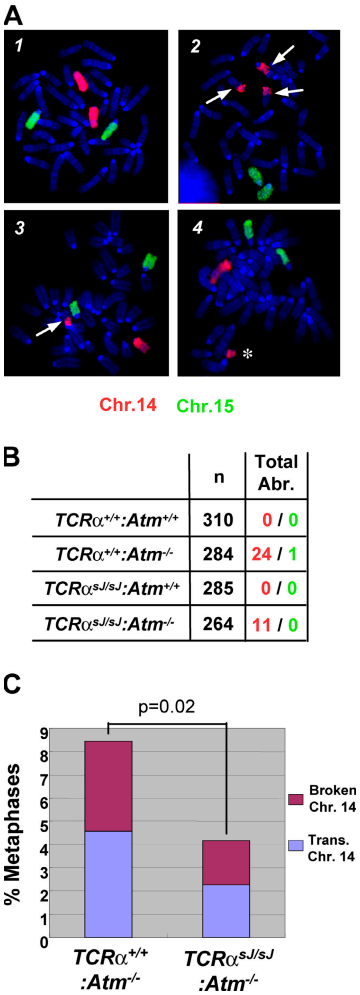

Figure 5. Decreased chromosome 14 breaks and aberrant rearrangements in $TCR\alpha^{sJ/sJ}$:$Atm^{-/-}$ αβT cells. Metaphase WCP analysis of wild-type ($TCR\alpha^{+/+}$:$Atm^{+/+}$), ATM-deficient ($TCR\alpha^{+/+}$:$Atm^{-/-}$), TCRα$^{sJ/sJ}$ ($TCR\alpha^{sJ/sJ}$:$Atm^{+/+}$), and ATM-deficient TCRα$^{sJ/sJ}$ ($TCR\alpha^{sJ/sJ}$:$Atm^{-/-}$) lymph node αβ T cells. Metaphases were hybridized to red chromosome 14 (TCRα/δ) and green chromosome 15 (control) WCPs. (A) Metaphases from $TCR\alpha^{sJ/sJ}$:$Atm^{+/+}$ (panel 1), $TCR\alpha^{sJ/sJ}$:$Atm^{-/-}$ (panel 2), and $TCR\alpha^{+/+}$:$Atm^{-/-}$ (panels 3 and 4) αβ T cells. Chromosome translocations (arrows) and broken chromosomes (asterisk) are indicated. (B) Number of metaphases with chromosome 14 (red) or 15 (green) breaks or translocations. (C) Percentage of $TCR\alpha^{+/+}$:$Atm^{-/-}$ and $TCR\alpha^{sJ/sJ}$:$Atm^{-/-}$ metaphases with chromosome 14 breaks (red) or translocations (blue). Datasets are pooled from two individual experiments.

unrepaired CEs accumulate in these cells due, at least in part, to their loss from postcleavage complexes (28). Although it is not possible to perform similar types of analyses on developing lymphocytes, we suspect that the loss of CEs from postcleavage complexes also contributes to the coding joint defect observed in developing ATM-deficient lymphocytes in vivo.

Cytogenetic analyses revealed that 2% of proliferating $TCR\alpha^{sJ/sJ}$:$Atm^{-/-}$ αβ T cells have chromosome 14 translocations, suggesting that some Jα CEs are aberrantly resolved (Fig. 5). In agreement, cytogenetic analyses of ATM-deficient

AMuLV pre–B cells that had undergone recombination revealed that 1.5% had chromosomal translocations involving the retroviral recombination substrate CEs (28). However, Southern blot analysis of clones revealed that 14% of the retroviral substrates had aberrantly resolved CEs (28). This difference (1.5% by cytogenetic and 14% by clonal analysis) is caused by the inability of cytogenetic approaches to detect many chromosomal deletions and inversions involving the retroviral substrate (28). By analogy, we would expect that the true fraction of *TCRα$^{sJ/sJ}$:Atm$^{-/-}$* αβ T cells with aberrant TCRα^{sJ} allele rearrangements is likely greater than the 2% with translocations detected using cytogenetic approaches (Fig. 5).

Defects in coding joint formation were found at both Ig and TCR loci and during D to J and V to DJ rearrangements in developing B and T cells, yet the lymphopenia of ATM deficiency is more profound in the T cell than the B cell compartment (15). It is possible that distinct features of TCR gene assembly contribute to the more pronounced T lymphopenia of ATM deficiency. The generation of translocations or large chromosomal deletions or inversions involving an antigen receptor locus would likely prevent subsequent rearrangements. Inactivation of a single allele in this manner would require the cell to generate an in-frame rearrangement on the alternate allele if it is to continue development, whereas inactivation of both alleles would preclude any further development. The developmental impact of such a defect should be greatest for loci that must undergo multiple rearrangements, as each additional rearrangement increases the possibility of inactivating the allele. In this regard, it is notable that in ATM-deficient mice the most profound block in T cell development occurs at the DP thymocyte stage, where TCRα chain genes are being assembled and expressed (12).

Developing T cells must assemble TCRα chain genes that are in frame and encode TCRα chains that form nonautoreactive αβ TCRs capable of positive selection. Most randomly generated αβ TCRs are not capable of mediating positive selection (35–37). The large Vα and Jα gene segment clusters are positioned such that all Vα to Jα rearrangements occur by deletion (31). Thus, VJα rearrangements that are not in frame, or that are in frame but do not encode a TCRα chain that forms a selectable αβ TCR, can be replaced through rearrangement of an upstream Vα to a downstream Jα gene segment on the same allele. In addition, TCRα chains that form autoreactive αβ TCRs can, in some instances, be similarly replaced, rescuing the cell from negative selection (38–40). These revision rearrangements proceed in an orderly fashion using progressively more 3′ Jα gene segments in the locus (32, 33). That most developing DP thymocytes must undergo multiple Vα to Jα rearrangements on each allele, as they attempt to generate a selectable αβ TCR, is supported by the defect in positive selection observed in *TCRα$^{sJ/sJ}$* mice (30).

A recent modeling study predicted that, on average, each TCRα allele undergoes five Vα to Jα rearrangements in developing thymocytes (41). In contrast, the TCRα^{sJ} allele can undergo only two Vα to Jα rearrangements. In this regard, it is notable that *TCRα$^{+/+}$:Atm$^{-/-}$* αβ T cells have twice as many chromosome 14 breaks and translocations as compared with *TCRα$^{sJ/sJ}$:Atm$^{-/-}$* αβ T cells (Fig. 5). Thus, there is a close correlation between the frequency of chromosome 14 breaks and translocations in ATM-deficient αβ T cells and the potential number of Vα to Jα rearrangements that these cells can make during thymocyte development. Collectively, these findings suggest that, in ATM-deficient cells, loci that undergo multiple rearrangements have an increased probability of generating a persistent unrepaired DSB or of sustaining an aberrant rearrangement, both of which should inactivate the allele and prevent further rearrangements.

What is the developmental impact of TCRα locus inactivation in ATM-deficient thymocytes? Although it is not possible to answer this question with certainty, an estimate of the potential developmental impact can be made. In ATM-deficient AMuLV pre–B cells, ∼14% of rearrangements lead to CEs that are aberrantly resolved in ways (translocations, deletions, and inversions) that would inactivate an antigen receptor locus (28). If 14% of TCRα gene rearrangements are also resolved aberrantly and an average of five Vα to Jα rearrangements occur on each TCRα allele, then on average there would be a 53% ($1 - 0.86^5$) possibility that a single TCRα allele would be inactivated in developing ATM-deficient DP thymocytes. Furthermore, approximately one third ($0.53 \times 0.53 = 0.28$) of ATM-deficient DP thymocytes would be expected to inactivate both TCRα alleles, precluding further development of these cells.

In addition to unrepaired TCRα CEs, unrepaired TCRβ chain gene CEs are also found in ATM-deficient thymocytes (Fig. 1 E). Thus, defects in TCRβ chain gene assembly may also contribute to the T lymphopenia of ATM deficiency. However, the only constraint on TCRβ chain gene assembly is that it must be in frame and encode a TCRβ chain that can form a pre-TCR (42). As a result, it is possible that developing thymocytes may undergo fewer TCRβ chain gene rearrangements than TCRα chain gene rearrangements. Moreover, the developmental impact of defects in TCRβ chain gene assembly may be blunted by the cellular expansion that occurs during the DN to DP transition (42). In contrast, positive selection is not accompanied by a substantial cellular expansion that could compensate for defects in TCRα chain gene assembly in ATM-deficient thymocytes.

Defects in coding joint formation during IgH and IgLκ chain gene assembly were also found in developing ATM-deficient B cells (Fig. 2 C), yet B cell development is minimally compromised in ATM-deficient mice (15). Like TCRβ chain gene assembly, IgH chain genes need only to be in frame and encode an IgH chain that can form a pre–B cell receptor (BCR) (43, 44). Furthermore, the pro– to pre–B cell transition is accompanied by a cellular expansion that could compensate for defects in IgH chain gene assembly (43, 44). IgL chain genes are assembled in pre–B cells, and they must encode an IgL chain that forms a nonautoreactive BCR (43, 44). As is the case for TCRα chain gene assembly, IgL chain gene assembly is not followed by a substantial cellular

expansion that could compensate for defects in this process (43, 44). Like the TCRα locus, the structure of the IgLκ locus permits VJκ rearrangements to be replaced with new VJκ rearrangements, on the same allele, as pre–B cells attempt to generate a nonautoreactive BCR (45). However, unlike the αβ TCR, there is no requirement for positive selection of the BCR. Thus, the additional constraint of positive selection may mandate more TCRα chain gene rearrangements in DP thymocytes than IgL chain gene rearrangements in pre–B cells and, as such, contribute to the more profound T cell lymphopenia of ATM deficiency.

It is also possible that developing T cells may have unique requirements for ATM function in addition to its role in antigen receptor gene assembly. For example, recent studies in macrophages have demonstrated that ATM deficiency leads to constitutive c-Jun N-terminal kinase (JNK) activation (46). JNK signals are involved in negative selection; therefore, if JNK activity is also perturbed in ATM-deficient thymocytes, this may contribute to the T lymphopenia of ATM deficiency (47). In addition, like ATM-deficient mice, mice that are deficient in both ATM and RAG eventually succumb to thymic lymphomas (21). However, these lymphomas do not have translocations involving the TCRα/δ locus (21). This demonstrates that ATM deficiency can promote thymocyte transformation through defects in processes other than the assembly of antigen receptor genes. Therefore, although we demonstrate unequivocally that ATM-deficient lymphocytes have defects in V(D)J recombination, the relative contribution of these and other defects to the lymphoid phenotypes of A-T remains to be determined.

MATERIALS AND METHODS

Mice. All mice were bred and maintained under specific pathogen-free conditions at the Washington University School of Medicine and were handled in accordance with the guidelines set forth by the Division of Comparative Medicine of Washington University.

Southern blot analyses. Southern blot analyses of genomic DNA and PCR products were performed as previously described (30, 48). P8, the CαI probe, and the RAG-2 probe (PR2) have been previously described (49). PS6 is a 0.4-kb PCR fragment amplified from TCRα$^{sJ/sJ}$ genomic DNA using the PS6-1 and PS6-2 oligonucleotides (Table S1, available at http://www.jem.org/cgi/content/full/jem.20061460/DC1). For exonuclease V digestion, 15 μg of thymocyte DNA was treated with increasing concentrations of exonuclease V, using the manufacturer's buffer conditions (USB Corporation), for 1 h at 37°C before restriction enzyme digestion and Southern blot analyses. For mung bean nuclease assays, 15 μg of thymocyte DNA was digested with 12.5 U of mung bean nuclease (New England Biolabs, Inc.) in 200 μl using the manufacturer's buffer supplemented with 0.4 mM $ZnSO_4$ at 25°C for 1 h before treatment with exonuclease V, as described in this section.

Quantification of Southern blot fragments. Quantifications of Southern blot fragments were performed on a PhosphorImager (Storm 840; GE Healthcare) using ImageQuant software (GE Healthcare). The percentage of TCRα^{sJ} alleles with unrepaired Jα56 CEs was calculated from the Southern blot of *StuI*-digested DNA probed with the CαI probe (Fig. 4 B) or PR2 as a DNA loading control (Fig. 4 B).

The following formula was used to determine the percentage of TCRα^{sJ} allele Jα56 CEs:

$$\frac{J\alpha 56CE^{Thy}/R2^{Thy}}{C\alpha I^{Kid}/R2^{Kid}} \times 100$$

The hybridization intensity of the CαI probe hybridizing the Jα56 CE fragment (Jα56CE^{Thy}) and PR2 hybridizing the RAG-2 gene fragment (R2^{Thy}) from *TCRα$^{sJ/sJ}$:Atm$^{-/-}$* thymus DNA is used. In addition, the hybridization intensity of the CαI probe hybridizing the germline TCRα^{sJ} allele fragment (CαI^{Kid}) and PR2 hybridizing the RAG-2 gene fragment (R2^{Kid}) from *TCRα$^{sJ/sJ}$:Atm$^{-/-}$* kidney DNA is used.

The percentage of TCRα^{sJ} alleles with unrepaired Jα61 CEs was similarly calculated from Southern blotting of *StuI*-digested DNA probed with PS6 (Fig. 4 B) using the following formula:

$$\frac{J\alpha 61CE^{Thy}/R2^{Thy}}{PS6^{Kid}/R2^{Kid}} \times 100$$

The hybridization intensity of PS6 hybridizing the Jα61 CE fragment (Jα61CE^{Thy}) from *TCRα$^{sJ/sJ}$:Atm$^{-/-}$* thymus DNA and the hybridization intensity of PS6 hybridizing the germline TCRα^{sJ} allele fragment (PS6^{Kid}) from *TCRα$^{sJ/sJ}$:Atm$^{-/-}$* kidney DNA are used. R2^{Thy} and R2^{Kid} are as described in this section.

The flowing formulas were used for quantifying the retention of Jα61 SEs and Jα56 CEs, respectively, after exonuclease V or mung bean nuclease and exonuclease V treatment:

$$\frac{J\alpha 61SE^{+ExoV}/GL^{+ExoV}}{J\alpha 61SE^{-ExoV}/GL^{-ExoV}} \times 100$$

and

$$\frac{J\alpha 56CE^{+ExoV}/GL^{+ExoV}}{J\alpha 56CE^{-ExoV}/GL^{-ExoV}} \times 100$$

The intensities of the Jα56 CE (Jα56CE), Jα61 SE (Jα61SE), or TCRα^{sJ} germline fragments in lanes that were either not treated ($^{-ExoV}$) or treated with different concentrations of exonuclease V ($^{+ ExoV}$) are used (Fig. 3 D; and Fig. 4, D and F).

LMPCR. LMPCR was performed as previously described (48). In brief, 4 μg of thymus DNA that was treated with the Klenow DNA polymerase (New England Biolabs, Inc.) in the presence of dNTP before ligation to the BW or ANC linker (48, 50). Heminested PCR was performed with Taq polymerase (Roche Molecular Systems, Inc.), according to the manufacturer's recommendation, using 1 mM $MgCl_2$. All primary PCRs were performed at 94°C for 5 min, followed by 17 cycles of 94°C for 30 s, 57°C for 30 s, and 72°C for 60 s. This was followed by a final incubation at 72°C for 7 min. All secondary PCRs were performed at 94°C for 5 min, followed by 23–36 cycles (Table S1) at 94°C for 30 s, 58°C for 30 s, and 72°C for 60 s. This was followed by a final incubation at 72°C for 7 min. Primer sequences are provided in Table S1. Oligonucleotides used as probes for PCR products are also listed in Table S1. IL-2 control PCR was performed as previously described (32).

Flow cytometric cell sorting. To purify CD25$^+$ DN thymocytes, total thymocytes were depleted with CD4- or CD8-expressing cells using magnetic beads, according to the manufacturer's instruction (Dynal), followed by flow cytometric purification of CD25$^+$ DN thymocytes (FACSDiva; Beckton Dickinson) using PE-Cy7–conjugated anti-CD25 (BD Biosciences). The resulting cells were >95% CD25$^+$ DN thymocytes. DP thymocytes were purified to >95% purity by flow cytometric cell sorting using FITC-conjugated anti-CD8 and PE-Cy7–conjugated anti-CD4 (BD Biosciences).

Metaphase WCP analysis. Metaphases were prepared from ConA-stimulated peripheral T cells, as previously described (28). Fluorescent in situ hybridization of metaphase chromosomes using the mouse WCPs (Applied Spectral Imaging) for chromosomes 14 (red) and 15 (green) were performed using the manufacturer's recommended procedure. In brief, denatured probes were allowed to reanneal at 37°C for 20 min and were hybridized to

denatured chromosomes for 16 h in a humidified chamber at 37°C. Stringency washing was done in 0.4× SSC at 70°C for 4 min, followed by 4× SSC/0.1% Tween 20. DAPI-counterstained slides were mounted in antiquench mount (Vectashield; Vector Laboratories) and analyzed on an epifluorescence microscope (Axioplan 2ie; Carl Zeiss MicroImaging, Inc.). Image acquisition and processing was done using ISIS software (Metasystems).

Online supplemental material. Table S1 presents a list of oligonucleotides used for LMPCR and probes. For each SE or CE LMPCR, the allele-specific oligonucleotides used as PCR primers or Southern probes are grouped with their names and sequences indicated. For TCRα locus LMPCR, the primers used for detecting SEs and CEs in the wild-type TCRα locus ($TCR\alpha^{+}$) or $TCR\alpha^{sJ}$ locus ($TCR\alpha^{sJ}$) are grouped, respectively. The cycle numbers for the primary and secondary reactions of the heminested PCR are also indicated alongside the allele-specific primers that were used. Primers A, B, and C are linker-specific primers. PS6-1 and PS6-2 are used to amplify PS6 for thymocyte DNA Southern analyses. Online supplemental material is available at http://www.jem.org/cgi/content/full/jem.20061460/DC1.

We thank Drs. Andrea Bredemeyer and Michael Krangel, and Beth Helmink for critical review of the manuscript.

B.P. Sleckman is supported by National Institutes of Health (NIH) grants AI47829 and AI49934 and American Cancer Society grant RSG-05-070-01-LIB. T.K. Pandita is supported by NIH grants NS34746 and CA10445. C.H. Bassing is a Pew Scholar. C.-Y. Huang is supported by a postdoctoral training grant from the NIH. Mice were housed in a facility supported by National Center for Research Resources grant RR012466.

The authors have no conflicting financial interests.

Submitted: 10 July 2006
Accepted: 19 January 2007

Note added in proof. Since the acceptance of this manuscript, another paper has appeared that also reports an increase in TCRα CEs in ATM-deficient mice (Vacchio, M.S., A. Olaru, F. Livak, and R.J. Hodes. 2007. *Proc. Natl. Acad. Sci. USA.* 104:6323–6328).

REFERENCES

1. Tonegawa, S. 1983. Somatic generation of antibody diversity. *Nature.* 302:575–581.
2. Oettinger, M.A. 1999. V(D)J recombination: on the cutting edge. *Curr. Opin. Cell Biol.* 11:325–329.
3. Gellert, M. 2002. V(D)J recombination: rag proteins, repair factors, and regulation. *Annu. Rev. Biochem.* 71:101–132.
4. Schatz, D.G. 2004. Antigen receptor genes and the evolution of a recombinase. *Semin. Immunol.* 16:245–256.
5. Bassing, C.H., and F.W. Alt. 2004. The cellular response to general and programmed DNA double strand breaks. *DNA Repair (Amst.).* 3:781–796.
6. Durocher, D., and S.P. Jackson. 2001. DNA-PK, ATM and ATR as sensors of DNA damage: variations on a theme? *Curr. Opin. Cell Biol.* 13:225–231.
7. Kastan, M.B., and D.S. Lim. 2000. The many substrates and functions of ATM. *Nat. Rev. Mol. Cell Biol.* 1:179–186.
8. Pandita, T.K. 2003. A multifaceted role for ATM in genome maintenance. *Expert Rev. Mol. Med.* 2003:1–21.
9. Shiloh, Y. 2003. ATM and related protein kinases: safeguarding genome integrity. *Nat. Rev. Cancer.* 3:155–168.
10. Lavin, M.F., and Y. Shiloh. 1997. The genetic defect in ataxia-telangiectasia. *Annu. Rev. Immunol.* 15:177–202.
11. Taylor, A.M., J.A. Metcalfe, J. Thick, and Y.F. Mak. 1996. Leukemia and lymphoma in ataxia telangiectasia. *Blood.* 87:423–438.
12. Matei, I.R., C.J. Guidos, and J.S. Danska. 2006. ATM-dependent DNA damage surveillance in T-cell development and leukemogenesis: the DSB connection. *Immunol. Rev.* 209:142–158.
13. Borghesani, P.R., F.W. Alt, A. Bottaro, L. Davidson, S. Aksoy, G.A. Rathbun, T.M. Roberts, W. Swat, R.A. Segal, and Y. Gu. 2000. Abnormal development of Purkinje cells and lymphocytes in Atm mutant mice. *Proc. Natl. Acad. Sci. USA.* 97:3336–3341.
14. Elson, A., Y. Wang, C.J. Daugherty, C.C. Morton, F. Zhou, J. Campos-Torres, and P. Leder. 1996. Pleiotropic defects in ataxia-telangiectasia protein-deficient mice. *Proc. Natl. Acad. Sci. USA.* 93:13084–13089.
15. Xu, Y., T. Ashley, E.E. Brainerd, R.T. Bronson, M.S. Meyn, and D. Baltimore. 1996. Targeted disruption of ATM leads to growth retardation, chromosomal fragmentation during meiosis, immune defects, and thymic lymphoma. *Genes Dev.* 10:2411–2422.
16. Barlow, C., S. Hirotsune, R. Paylor, M. Liyanage, M. Eckhaus, F. Collins, Y. Shiloh, J.N. Crawley, T. Ried, D. Tagle, and A. Wynshaw-Boris. 1996. Atm-deficient mice: a paradigm of ataxia telangiectasia. *Cell.* 86:159–171.
17. Matei, I.R., R.A. Gladdy, L.M. Nutter, A. Canty, C.J. Guidos, and J.S. Danska. 2006. ATM deficiency disrupts TCRα locus integrity and the maturation of CD4+CD8+ thymocytes. *Blood.* 109:1887–1896.
18. Liyanage, M., Z. Weaver, C. Barlow, A. Coleman, D.G. Pankratz, S. Anderson, A. Wynshaw-Boris, and T. Ried. 2000. Abnormal rearrangement within the α/δ T-cell receptor locus in lymphomas from Atm-deficient mice. *Blood.* 96:1940–1946.
19. Chao, C., E.M. Yang, and Y. Xu. 2000. Rescue of defective T cell development and function in Atm−/− mice by a functional TCR alpha beta transgene. *J. Immunol.* 164:345–349.
20. Liao, M.J., and T. Van Dyke. 1999. Critical role for Atm in suppressing V(D)J recombination-driven thymic lymphoma. *Genes Dev.* 13:1246–1250.
21. Petiniot, L.K., Z. Weaver, C. Barlow, R. Shen, M. Eckhaus, S.M. Steinberg, T. Ried, A. Wynshaw-Boris, and R.J. Hodes. 2000. Recombinase-activating gene (RAG) 2-mediated V(D)J recombination is not essential for tumorigenesis in Atm-deficient mice. *Proc. Natl. Acad. Sci. USA.* 97:6664–6669.
22. Desiderio, S., W.C. Lin, and Z. Li. 1996. The cell cycle and V(D)J recombination. *Curr. Top. Microbiol. Immunol.* 217:45–59.
23. Schlissel, M., A. Constantinescu, T. Morrow, M. Baxter, and A. Peng. 1993. Double-strand signal sequence breaks in V(D)J recombination are blunt, 5′-phosphorylated, RAG-dependent, and cell cycle regulated. *Genes Dev.* 7:2520–2532.
24. Jacks, T., L. Remington, B.O. Williams, E.M. Schmitt, S. Halachmi, R.T. Bronson, and R.A. Weinberg. 1994. Tumor spectrum analysis in p53-mutant mice. *Curr. Biol.* 4:1–7.
25. Hirao, A., A. Cheung, G. Duncan, P.M. Girard, A.J. Elia, A. Wakeham, H. Okada, T. Sarkissian, J.A. Wong, T. Sakai, et al. 2002. Chk2 is a tumor suppressor that regulates apoptosis in both an ataxia telangiectasia mutated (ATM)-dependent and an ATM-independent manner. *Mol. Cell. Biol.* 22:6521–6532.
26. Hsieh, C.L., C.F. Arlett, and M.R. Lieber. 1993. V(D)J recombination in ataxia telangiectasia, Bloom's syndrome, and a DNA ligase I-associated immunodeficiency disorder. *J. Biol. Chem.* 268:20105–20109.
27. Perkins, E.J., A. Nair, D.O. Cowley, T. Van Dyke, Y. Chang, and D.A. Ramsden. 2002. Sensing of intermediates in V(D)J recombination by ATM. *Genes Dev.* 16:159–164.
28. Bredemeyer, A.L., G.G. Sharma, C.Y. Huang, B.A. Helmink, L.M. Walker, K.C. Khor, B. Nuskey, K.E. Sullivan, T.K. Pandita, C.H. Bassing, and B.P. Sleckman. 2006. ATM stabilizes DNA double-strand-break complexes during V(D)J recombination. *Nature.* 442:466–470.
29. Willerford, D.M., W. Swat, and F.W. Alt. 1996. Developmental regulation of V(D)J recombination and lymphocyte differentiation. *Curr. Opin. Genet. Dev.* 6:603–609.
30. Huang, C.Y., B.P. Sleckman, and O. Kanagawa. 2005. Revision of T cell receptor α chain genes is required for normal T lymphocyte development. *Proc. Natl. Acad. Sci. USA.* 102:14356–14361.
31. Glusman, G., L. Rowen, I. Lee, C. Boysen, J.C. Roach, A.F. Smit, K. Wang, B.F. Koop, and L. Hood. 2001. Comparative genomics of the human and mouse t cell receptor loci. *Immunity.* 15:337–349.
32. Huang, C., and O. Kanagawa. 2001. Ordered and coordinated rearrangement of the TCR α locus: role of secondary rearrangement in thymic selection. *J. Immunol.* 166:2597–2601.
33. Guo, J., A. Hawwari, H. Li, Z. Sun, S.K. Mahanta, D.R. Littman, M.S. Krangel, and Y.W. He. 2002. Regulation of the TCRα repertoire by

the survival window of CD4(+)CD8(+) thymocytes. *Nat. Immunol.* 3:469–476.
34. Villey, I., D. Caillol, F. Selz, P. Ferrier, and J.P. de Villartay. 1996. Defect in rearrangement of the most 5′ TCR-Jα following targeted deletion of T early alpha (TEA): implications for TCR α locus accessibility. *Immunity.* 5:331–342.
35. Huesmann, M., B. Scott, P. Kisielow, and H. von Boehmer. 1991. Kinetics and efficacy of positive selection in the thymus of normal and T cell receptor transgenic mice. *Cell.* 66:533–540.
36. Sant'Angelo, D.B., B. Lucas, P.G. Waterbury, B. Cohen, T. Brabb, J. Goverman, R.N. Germain, and C.A. Janeway Jr. 1998. A molecular map of T cell development. *Immunity.* 9:179–186.
37. Correia-Neves, M., C. Waltzinger, D. Mathis, and C. Benoist. 2001. The shaping of the T cell repertoire. *Immunity.* 14:21–32.
38. Buch, T., F. Rieux-Laucat, I. Forster, and K. Rajewsky. 2002. Failure of HY-specific thymocytes to escape negative selection by receptor editing. *Immunity.* 16:707–718.
39. McGargill, M.A., J.M. Derbinski, and K.A. Hogquist. 2000. Receptor editing in developing T cells. *Nat. Immunol.* 1:336–341.
40. Wang, F., C.Y. Huang, and O. Kanagawa. 1998. Rapid deletion of rearranged T cell antigen receptor (TCR) Vα-Jα segment by secondary rearrangement in the thymus: role of continuous rearrangement of TCR α chain gene and positive selection in the T cell repertoire formation. *Proc. Natl. Acad. Sci. USA.* 95:11834–11839.
41. Warmflash, A., and A.R. Dinner. 2006. A model for TCR gene segment use. *J. Immunol.* 177:3857–3864.
42. von Boehmer, H., and H.J. Fehling. 1997. Structure and function of the pre-T cell receptor. *Annu. Rev. Immunol.* 15:433–452.
43. Rajewsky, K. 1996. Clonal selection and learning in the antibody system. *Nature.* 381:751–758.
44. Hardy, R.R., and K. Hayakawa. 2001. B cell development pathways. *Annu. Rev. Immunol.* 19:595–621.
45. Jankovic, M., R. Casellas, N. Yannoutsos, H. Wardemann, and M.C. Nussenzweig. 2004. RAGs and regulation of autoantibodies. *Annu. Rev. Immunol.* 22:485–501.
46. Schneider, J.G., B.N. Finck, J. Ren, K.N. Standley, M. Takagi, K.H. Maclean, C. Bernal-Mizrachi, A.J. Muslin, M.B. Kastan, and C.F. Semenkovich. 2006. ATM-dependent suppression of stress signaling reduces vascular disease in metabolic syndrome. *Cell Metab.* 4:377–389.
47. Rincon, M., A. Whitmarsh, D.D. Yang, L. Weiss, B. Derijard, P. Jayaraj, R.J. Davis, and R.A. Flavell. 1998. The JNK pathway regulates the in vivo deletion of immature $CD4^+CD8^+$ thymocytes. *J. Exp. Med.* 188:1817–1830.
48. Tillman, R.E., A.L. Wooley, M.M. Hughes, T.D. Wehrly, W. Swat, and B.P. Sleckman. 2002. Restrictions limiting the generation of DNA double strand breaks during chromosomal V(D)J recombination. *J. Exp. Med.* 195:309–316.
49. Livak, F., H.T. Petrie, I.N. Crispe, and D.G. Schatz. 1995. In-frame TCR δ gene rearrangements play a critical role in the αβ/γδ T cell lineage decision. *Immunity.* 2:617–627.
50. Livak, F., and D.G. Schatz. 1997. Identification of V(D)J recombination coding end intermediates in normal thymocytes. *J. Mol. Biol.* 267:1–9.